

---

This is an electronic reprint of the original article.  
This reprint may differ from the original in pagination and typographic detail.

Khabushev, Eldar M.; Krasnikov, Dmitry V.; Goldt, Anastasia E.; Fedorovskaya, Ekaterina O.; Tsapenko, Alexey P.; Zhang, Qiang; Kauppinen, Esko I.; Kallio, Tanja; Nasibulin, Albert G.  
**Joint effect of ethylene and toluene on carbon nanotube growth**

*Published in:*  
Carbon

*DOI:*  
[10.1016/j.carbon.2021.12.052](https://doi.org/10.1016/j.carbon.2021.12.052)

Published: 15/04/2022

*Document Version*  
Peer-reviewed accepted author manuscript, also known as Final accepted manuscript or Post-print

*Published under the following license:*  
CC BY-NC-ND

*Please cite the original version:*  
Khabushev, E. M., Krasnikov, D. V., Goldt, A. E., Fedorovskaya, E. O., Tsapenko, A. P., Zhang, Q., Kauppinen, E. I., Kallio, T., & Nasibulin, A. G. (2022). Joint effect of ethylene and toluene on carbon nanotube growth. *Carbon*, 189, 474-483. <https://doi.org/10.1016/j.carbon.2021.12.052>

---

This material is protected by copyright and other intellectual property rights, and duplication or sale of all or part of any of the repository collections is not permitted, except that material may be duplicated by you for your research use or educational purposes in electronic or print form. You must obtain permission for any other use. Electronic or print copies may not be offered, whether for sale or otherwise to anyone who is not an authorised user.

# Joint effect of ethylene and toluene on carbon nanotube growth

Eldar M. Khabushev<sup>1,2</sup>, Dmitry V. Krasnikov<sup>1</sup>, Anastasia E. Goldt<sup>1</sup>, Ekaterina O. Fedorovskaya<sup>2</sup>, Alexey P. Tsapenko<sup>3</sup>, Qiang Zhang<sup>3</sup>, Esko I. Kauppinen<sup>3</sup>, Tanja Kallio<sup>2</sup> and Albert G. Nasibulin<sup>1,2\*</sup>

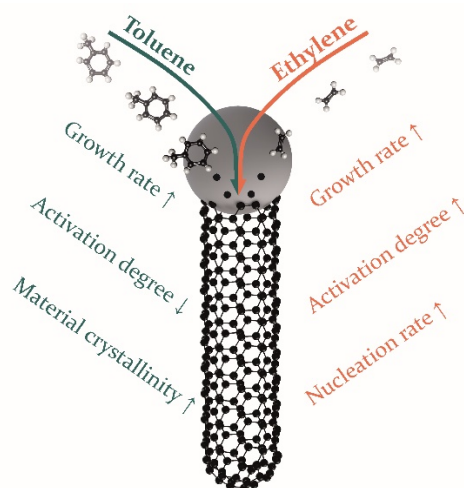
<sup>1</sup>Skolkovo Institute of Science and Technology, Nobel 3, 121205, Moscow, Russia

<sup>2</sup>Aalto University, School of Chemical Engineering, Kemistintie 1, 02015, Espoo, Finland

<sup>3</sup>Aalto University, Department of Applied Physics, Puumiehenkuja 2, 00076 Espoo, Finland

\*Corresponding author: [a.nasibulin@skoltech.ru](mailto:a.nasibulin@skoltech.ru)

## Graphical Abstract



## Abstract

This work contributes to the understanding of single-walled carbon nanotube synthesis by an aerosol CVD method using ethylene and toluene as a hybrid carbon source. We evaluated an extensive set of synthesis conditions revealing the role of ferrocene, toluene, and ethylene. We found the fundamental role of ethylene promoting nanotube nucleation and catalyst activation degree at all the concentrations studied, and enhancing nanotube growth at low ethylene content. We observed the interplay effect of toluene and ethylene concentrations on the nanotube growth rate, accompanied by the detrimental effect of toluene on catalyst activation degree. Nevertheless,

toluene apparently promotes nanotube crystallinity, increasing the film conductivity while used as an individual carbon source. Adjusting the ethylene and toluene concentrations, we produced carbon nanotube-based transparent and conductive films with an equivalent sheet resistance (at 90% transmittance at 550 nm wavelength) value of  $57 \Omega/\square$  at the synthesis yield of  $0.24 \text{ cm}^2 \cdot \text{L}^{-1}$ , which is at least two times higher than the results reported earlier.

**Keywords:** Aerosol CVD synthesis; Floating catalyst; Single-walled carbon nanotube; Equivalent sheet resistance.

## 1. Introduction

Thin films of single-walled carbon nanotubes (SWCNTs) are believed to be a prospective material for various applications including gas filtration [1], UV-protective membranes [2], thin-film transistors [3–5], bolometers and thermophones [6,7], transparent electrodes [8], and others [9]. In fact, SWCNTs have game-changing promise in electronic implementations since they are expected both to replace materials based on rare metals [10] (*e.g.* indium-tin-oxide) in transparent electronics and to boost the technology of flexible and stretchable devices due to their superior mechanical properties [11,12].

Among various synthesis approaches, an aerosol (a specific case of floating catalyst) chemical vapor deposition (CVD) [13] method is one of the most technologically promising and effective techniques for direct large-scale production of nanotube-based transparent and conductive films (TCFs), bypassing time and recourse intermediate dispersion and purification procedures [14,15]. Besides, the aerosol CVD provides pathways for *in situ* control over nanotube characteristics and process efficiency [16] achieved by implementation of growth promoters, specific oxidizing agents, and by selection of carbon feedstock [17]. For example, a small amount of  $\text{CO}_2$  additive, as an oxidizing agent, governs the diameter and length of SWCNTs in the CO-based process [18], sulfur addition to hydrocarbon-based synthesis effectively promotes nanotube growth (synthesis productivity) [19], while  $\text{NH}_3$  and oxygen-based compounds may specifically etch nanotubes with certain chirality [20]. Several research works provided evidence for feedstock-

dependent nanotube nucleation [21] and growth [22] (*e.g.*, preferential growth of near-armchair chirality with ethanol and toluene [23]), highlighting the pivotal role of carbon source in the nanotube synthesis.

Fine-tuning of microscopic nanotube characteristics (length, defectiveness, *etc.*) enables control over macroscopic features of their films, in particular their optoelectrical properties [24]. Thus, SWCNT-based TCFs produced by the aerosol CVD method are considered as the superior one and might, in theory, exhibit performance comparable to the widely used indium-tin-oxide [25]. However, the productive synthesis of high-performance nanotube films is still challenging due to limited residence time and fundamental constraints associated with gas-phase aggregation (bundling) [26]. From this perspective, advanced control over nanotube growth, particularly high-growth-rate synthesis of non-defective SWCNTs, is a key for further advancement in the field.

In fact, the implementation of several carbon sources was shown to enable more delicate control over the aerosol CVD nanotube growth [27]. For instance, addition of ethylene in the presence of carbon monoxide enhances nanotube yield (compared to the pure carbon monoxide system), preserving quality and conductive characteristics of the material [28]. At the same time, a combination of toluene and ethylene enabled the fabrication of films of long “carbon-welded” SWCNTs with transparent and conductive performance (equivalent sheet resistance) of  $25 \Omega/\square$  at 90% transmittance in the middle of visible wavelength range [29]. This result is close to the performance of commercially available indium-tin-oxide, though the time stability of the film and productivity of the process were extremely low. Moreover, recent advances in nanotube-based films produced only with ethylene [30] or toluene [31] indicate the attainability of high-performance TCF production with elevated yield and highlight the relevance of further research of the perspective hybrid system. Nevertheless, a lack of understanding of the mutual impact of various carbon sources on the SWCNT growth inhibits the development of synthetic hydrocarbon-based systems in particular and the synthesis of nanotubes in general.

This work closes this gap and reveals the joint effect of two carbon sources (ethylene and toluene) on the SWCNT synthesis in the aerosol CVD method. We examine the effect of SWCNT parameters on the resulted properties of transparent and conductive SWCNT films with a focus on the productivity of the process. In addition, we discuss the roles of particular feedstock in nanotube growth and provide a critical assessment of the system. We believe this work is to guide the path towards the advanced performance of SWCNT films in optoelectronic applications.

## 2. Experimental

### 2.1 Sample fabrication

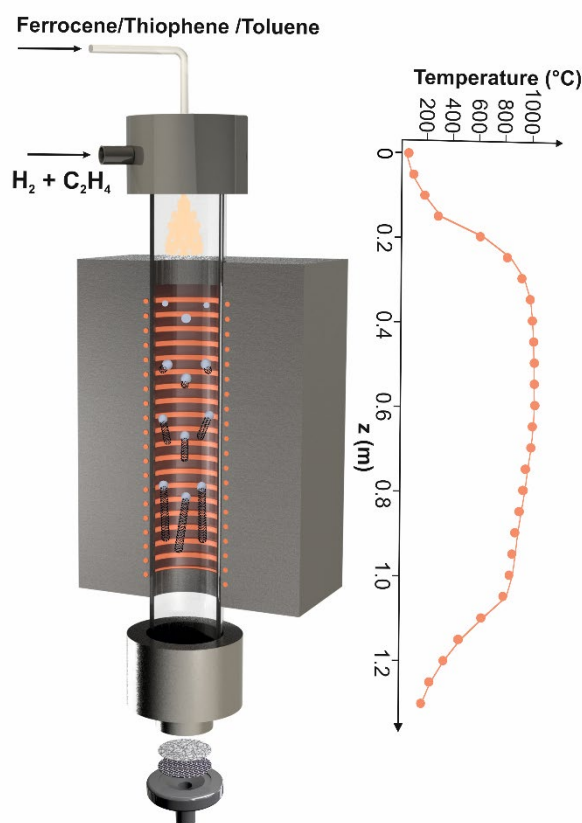


**Figure 1.** Scheme of aerosol CVD reactor and measured temperature profile along the reactor tube centerline ( $z$ -axis). The origin corresponds to the tube inlet.

We synthesized SWCNTs using an aerosol (floating-catalyst) CVD reactor (**Figure 1**) operating at atmospheric pressure, which consisted of a quartz tube (inner diameter 44 mm, length 1.3 m) placed in the vertical tubular furnace heated to set temperature of 1000°C. The measured length of the reactor isothermal zone ( $\pm 10^\circ\text{C}$ ) was of 40 cm. Hydrogen (Linde Gas, 5.0 purity) with a fixed flow rate of 7.2 slpm was used as carrier gas to prevent non-catalytic hydrocarbon

pyrolysis [32]. Small amount of ethylene (Linde Gas, 4.5 purity) was added to hydrogen. Ferrocene (Sigma-Aldrich, 98%) and thiophene (Sigma-Aldrich, 99%) – an iron-based catalyst precursor and a sulfur-containing promoter – were dissolved in toluene (Sigma-Aldrich,  $\geq 99.9\%$ ). The solution was evaporated using SONOZAP Ultrasonic Atomizer and then injected into the reactor using a high-precision syringe pump (NE-1000, New Era Instruments). Carbon nanotubes grown in the gas phase were collected at the outlet of the reactor on a nitrocellulose membrane filter (MF-Millipore, 0.45  $\mu\text{m}$  pore size) with a diameter of filtration area of 22 mm. The collected films were dry-transferred [33] on a glass slide for subsequent characterization.

## 2.2 Experimental conditions

We prepared several toluene solutions with ferrocene concentrations in the range from 0.125 to 2 wt%; the thiophene to ferrocene mass ratio was kept constant at 0.8 (corresponding to Fe/S mass ratio equal to unity while the molar ratio was 1.77). To thoroughly investigate the influence of synthesis parameters on the characteristics of produced nanotube films, we performed an extensive set of experiments varying ethylene concentration and adjusting the solution feed rate. This approach allowed us to examine the effect of every particular synthesis parameter (ferrocene feed rate, toluene, and ethylene concentration) while others being fixed (**Table 1**).

**Table 1.** Synthesis conditions used for nanotube production. Here, ferrocene concentration in the solution is denoted as  $X_{\text{ferrocene}}$ . Toluene ( $X_{\text{toluene}}$ ) and ethylene ( $X_{\text{ethylene}}$ ) concentrations were calculated as a volumetric fraction in terms of ideal gas assumption. Ferrocene feed rate was calculated as a product of its concentration and solution feed rate.

$X_{\text{ferrocene}}$ (wt%)	Solution feed rate ( $\mu\text{l}/\text{min}$ )	$X_{\text{ethylene}}$ (vol%)	$X_{\text{toluene}}$ (vol%)	Ferrocene feed rate ( $\mu\text{g}/\text{min}$ )
2	3.75, 6.25, 12.5, 18.75	0–3	0.01, 0.02, 0.04, 0.06	65
1*	7.5, 12.5, 25, 37.5		0.02, 0.04, 0.08, 0.11	108
0.5	15, 25, 50, 75		0.05, 0.08, 0.15, 0.23	217
0.25	30, 50, 100, 150		0.09, 0.15, 0.30, 0.46	325
0.125	60, 100, 200, 300		0.18, 0.30, 0.61, 0.91	

\*For 1 wt% catalyst precursor concentration solution, additional experiments were carried out at solution feed rates of 5  $\mu\text{l}/\text{min}$  in order to optimize equivalent sheet resistance of the films.

It should be noted that toluene was used as a solvent for the catalyst precursor and promoter, so we were not able to study the process in absent of toluene; though during some experiments its concentration was as low as 0.01 vol%.

### 2.3 Sample characterization

We utilized absorption spectroscopy (Perkin Elmer UV-vis-NIR spectrophotometer Lambda 1050) and FTIR spectroscopy (Bruker FTIR ALPHA II tool) to estimate the yield and mean diameter of produced SWCNTs. Mean diameter was recalculated according to the procedure described in details elsewhere [34]. Briefly, the diameter distribution was derived from the position and shape of S<sub>11</sub> transition peak according to reference data provided in the Kataura plot [35]. The yield was calculated as a rate (per unit time  $t$ ) of 90% transmittance ( $T$ ) film collection normalized to reactor flow rate and filter collection area ( $d$  is the diameter of an active part of the filter):

$$Yield [cm^2 \cdot L^{-1}] = \frac{\log_{0.9}(T)}{t[\min] \cdot flow\ rate [slpm]} \cdot \frac{\pi (d[cm])^2}{4}$$

The quality of carbon nanotubes was evaluated by Raman spectroscopy (Renishaw inVia Confocal Raman Microscope) equipped with 532 nm excitation laser and 100x objective. Spectra were collected at the laser power below 1 mW with 0.2 s exposure time and >100 frames averaging; a laser beam spot size was estimated to be several micrometers. Measurements were repeated at least in three positions of a sample and then averaged.

To measure the sheet resistance of the films, we used a four-probe station Jandel RM3000. For each of the films, the measurements were repeated five times (at various angles between a film and probes), while the obtained values were averaged. The current was varied from 0.01 to 1 mA depending on a sample conductivity (current was adjusted to keep measured voltage drop in the range above 10 mV). The mean deviation of sheet resistance from average was estimated to be *c.a.* 9.6%.

The SWCNT length distribution was studied by scanning electron microscopy (SEM, JEOL JSM-7001F), while the morphology of the samples was investigated by transmission

electron microscopy (TEM) using 120 kV FEI Tecnai 12 and JEOL-JEM-2800 tools. For SEM and TEM imaging, SWCNTs were deposited on Si/SiO<sub>2</sub> and Lacey carbon Cu-300 grid, correspondingly, directly from the gas phase by placing the substrates on a nitrocellulose filter within the nanotube aerosol flow.

The doping procedure was performed by dip-coating the SWCNT films into 15 mM ethanol solution of H<sub>2</sub>AuCl<sub>4</sub> (99.9% Acros) using Xdip-MV1 Apex Instruments at 100 mm/min speed. The films were remained inside the solution for 20 seconds and pulled up at a constant speed of 100 mm/min.

### **3. Results and discussion**

The systematic variation of synthesis parameters and comprehensive characterization of produced samples allowed us to get insights into the influence of synthesis parameters on the characteristics of the produced nanotubes and their randomly-oriented films (Figure S9). We evaluated the synthesis efficiency (Yield), nanotube structural properties ( $I_G/I_D$  describing nanotube quality), and transparent film quality factor ( $R_{90}$  is the equivalent sheet resistance at 90% transmittance at the wavelength of 550 nm) at every growth recipe studied. In particular, we focused on the mutual effects of catalyst and carbon feedstock concentration (feed rates) since these parameters primarily govern nanotube growth from nucleation to growth termination stage. However, as the dataset obtained ascribes influence of at least three linearly independent parameters (ferrocene feed rate, ethylene, and toluene concentrations), we first highlight the trends for each parameter varied alone (like a cut of a multidimensional space) to set the scene for complex analysis.

#### *3.1 The effect of catalyst concentration*

The effects of catalyst precursor (ferrocene) feed rate [36], as well as the ways of catalyst nanoparticle production [37] and injection [38], were abundantly examined previously for the aerosol CVD method. In fact, the ferrocene feed rate regulates the kinetics of nanoparticle formation, which is governed by a complex coagulation process. Our results (**Figure 2a**) show the

SWCNT yield to dramatically grow with the increase in catalyst amount with an apparent reaction order with respect to ferrocene (reaction rate) of 2.5. This result highlights the non-linearity of the catalyst formation process and nanotube growth in general. It might also indicate the promoting effect of ferrocene hydrocarbon residuals on the nanotube growth efficiency [37]. We consider the ferrocene feed rate to determine the number of active sites (nanoparticles) of nanotube growth and, as a result, the productivity of the process. In fact, an increase in catalyst precursor concentration aggravates the nanotube agglomeration (bundling), affecting the morphology of the collected material (**Figure 2c-e**): we observed an increase in number of unused catalyst nanoparticles and an apparent growth of bundle diameter with ferrocene feed rate rise. Besides, we observed a relatively small fraction of pyrolytic carbon in the samples, that is also supported by typical Raman spectra presented in Figure S2 (low intensity and narrow D-band was observed). However, the nanotube bundling is considered as an unfavorable process for nanotube TCFs since it significantly increases absorption of material without a noticeable gain in electrical conductivity [26]. Indeed, we observed a negative effect of ferrocene feed rate on the quality of produced material and on its conductive characteristics (Figure S1). For this reason, in our research, we mainly investigated the performance of nanotube-based TCFs produced at relatively low ferrocene feed rates.

At the same time, the process of catalyst formation and, as follows, nucleation pattern could also be displayed on the diameter of produced nanotubes. Restoring SWCNT diameter distribution with the help of optical absorption spectroscopy ( $S_{11}$  peak position), we observed a slight rise in the mean nanotube diameter with ferrocene feed rate increase (**Figure 2b**). The observed trend is associated with the enhanced growth rate of catalyst particles preceding the nucleation stage. Indeed, the nanotube nucleation takes place in terms of continuous process of nanoparticle coagulation, while the nanotube diameter is proven to correlate with the size of the active catalyst particle [38] and most likely does not change in terms of steady growth [39]. We did not observe any change in the diameter distribution width (standard deviation) with ferrocene feed rate

variation; this fact indicates that nanotube nucleation is rather limited by agglomeration of Fe-based aerosol nanoparticles than carbon feedstock decomposition [40,41].

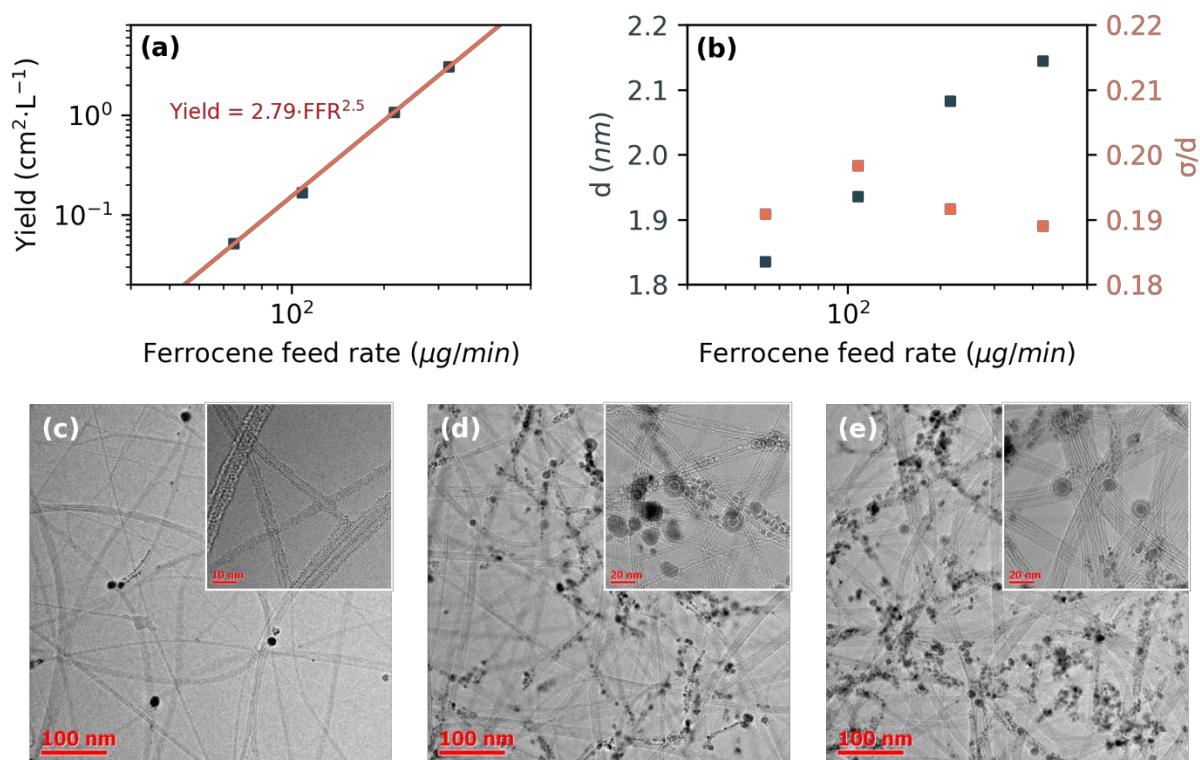


**Figure 2.** (a,b) – Ferrocene feed rate (FFR) effect on the synthesis productivity (yield) and nanotube diameter relation; (c-e) – TEM micrographs of nanotube samples fabricated at ferrocene feed rates of 108, 217 and 325 μg/min. The ethylene and toluene concentrations were fixed at 0.4 and 0.15 vol%, correspondingly. Here  $d$  and  $\sigma$  correspond to mean and standard deviation of SWCNT diameter distribution.

Thus, we observe the ferrocene concentration to show a complex impact on the growth process. While the intuitive direct relation between the catalyst amount and the yield is enhanced to the apparent reaction order with respect to ferrocene of 2.5, the ferrocene concentration manifests itself via a slight increase in the mean diameter of SWCNTs and declining trends in film conductivity and quality of the material.

### 3.2 The role of ethylene

Ethylene is known to be one of the most widely used carbon feedstocks for the synthesis of SWCNTs and carbon nanomaterials in general. This is due to its relatively low cost and low

toxicity (in contrast to carbon monoxide) and the promoting role of  $C_2H_x$  radicals in catalyst precursor decomposition and nanotube nucleation [22]. Previously, a control over nanotube diameter distribution by ethylene addition was reported for the toluene/ethylene hybrid system [42]. Our results (**Figure 3a**) support the previous findings, with a mean diameter being a linear function of ethylene concentration tuned in 1.3–2.2 nm range (**Figure 3b**), according to UV-vis-NIR spectra and also displayed by radial breathing modes in Raman spectra (Figure S2). Moreover, we observed a widening of nanotube diameter distribution (**Figure 3b**) with increase in ethylene concentration. Thus, ethylene addition results not only in the enhancement of the nucleation process (because ethylene is considered to decompose catalytically faster than toluene [22]) but also in a favorable effect on the catalyst activation degree (discussed below), since a broader range of catalyst nanoparticles is activated. On the contrary, we did not observe the same effect while increasing toluene concentration (Figure S3) that highlights the key role of ethylene in nucleation and fits well with feedstock dependence of this process.

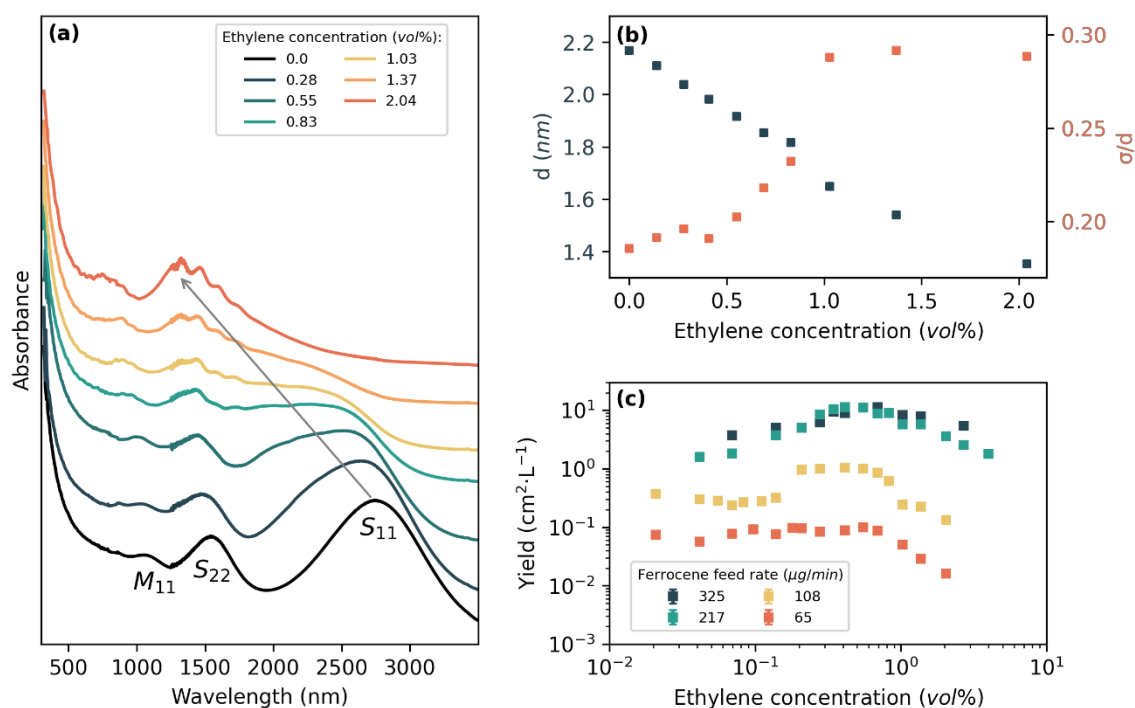


**Figure 3.** (a,b) – Evolution of optical absorption spectra and nanotube diameter distribution with ethylene concentration at fixed toluene concentration of 0.15 vol% and ferrocene feed rate of 65  $\mu g/min$ . Here,  $d$  and  $\sigma$

correspond to mean and standard deviation of diameter distribution. (c) – Synthesis productivity (yield) relation on ethylene concentration at fixed toluene concentration of 0.15 vol%.

Besides, we found the ethylene concentration to govern the productivity of the synthesis process in the whole ferrocene feed rate range investigated (**Figure 3c**). We observed a bell-shaped dependence of the yield on ethylene concentration with initial growth, the peak at *c.a.* 0.4 vol% followed by a steady decline. Surprisingly, we did not observe any significant yield enhancement at the optimal ethylene concentration while increasing ferrocene feed rate above 217  $\mu\text{g}/\text{min}$ , with the yield reaching maxima of  $\sim 11.5 \text{ cm}^2 \cdot \text{L}^{-1}$ . The observed saturation effect might be related to fundamental limitations associated with gas-phase nanotube bundling and the induced catalyst deactivation process. Nevertheless, the detailed study of this phenomenon is a subject of another study.

As a rule, a higher yield can be attributed either to an increase of nanotube growth rate (leading to longer SWCNTs) and/or to the enhanced catalyst activation degree (i.e., increase in the fraction of the active Fe particles) and/or to the formation of pyrolytic carbon (resulting in the drop of the material quality [24]). Evaluation of catalyst and amorphous carbon (found to be negligible, Figure S2) mass fractions might provide insights in catalyst activation degree and productivity, and reveal the role of ethylene. Unfortunately, employing low catalyst feed rates with a focus on transparent and conducting application of SWCNT films, we were not capable of performing TGA due to the relatively low mass yield of material. As an alternative, we coupled the results of film characterization techniques (optical absorption, Raman, and sheet resistance measurements) with the nanotube morphology studied by SEM and TEM (Figure S4-S6). The experiments were performed at a low ferrocene feed rate (43  $\mu\text{g}/\text{min}$ ) and toluene concentration of 0.015 vol% (corresponding to 5  $\mu\text{l}/\text{min}$  feed rate of 1 wt% ferrocene solution; Figure S7) and optimized reactor temperature of 1050°C (Figure S8). We operated with Yield as a quantitative parameter, which we believe, is projecting the catalyst activation degree with length/ $R_{90}$  taken into account.

**Figure 4** demonstrates the diverse ethylene effect on SWCNT film properties. Firstly, we found the ethylene not only to affect the synthesis yield (**Figure 4a**) but also to govern the nanotube quality (described by  $I_G/I_D$  ratio; **Figure 4b**) and film conductivity ( $R_{90}$ ; **Figure 4c**). Moreover, we observed the correlation between  $I_G/I_D$  and yield ethylene relations with  $I_G/I_D$  value rising from 40 to above 200 at 0.3-0.4 vol% ethylene concentration and subsequently declining at higher concentrations. At the same time, the  $R_{90}$  relation on ethylene concentration does not show any clear correlation with the yield, steadily declining at ethylene concentrations below 0.15 vol% and reaching minima of *c.a.*  $300 \Omega/\square$  with a further dramatic rise at higher concentrations. The lack of  $R_{90}$ -yield correlation could be attributed to the complexity of  $R_{90}$  parameter being a function of material quality/purity [43], bundling degree [26], nanotube length [44], *etc.* Overall, the ethylene improves  $R_{90}$  in two orders of magnitude and affects nanotube quality and process productivity proving, thereby, the fundamental role of ethylene as a carbon source for SWCNT growth.

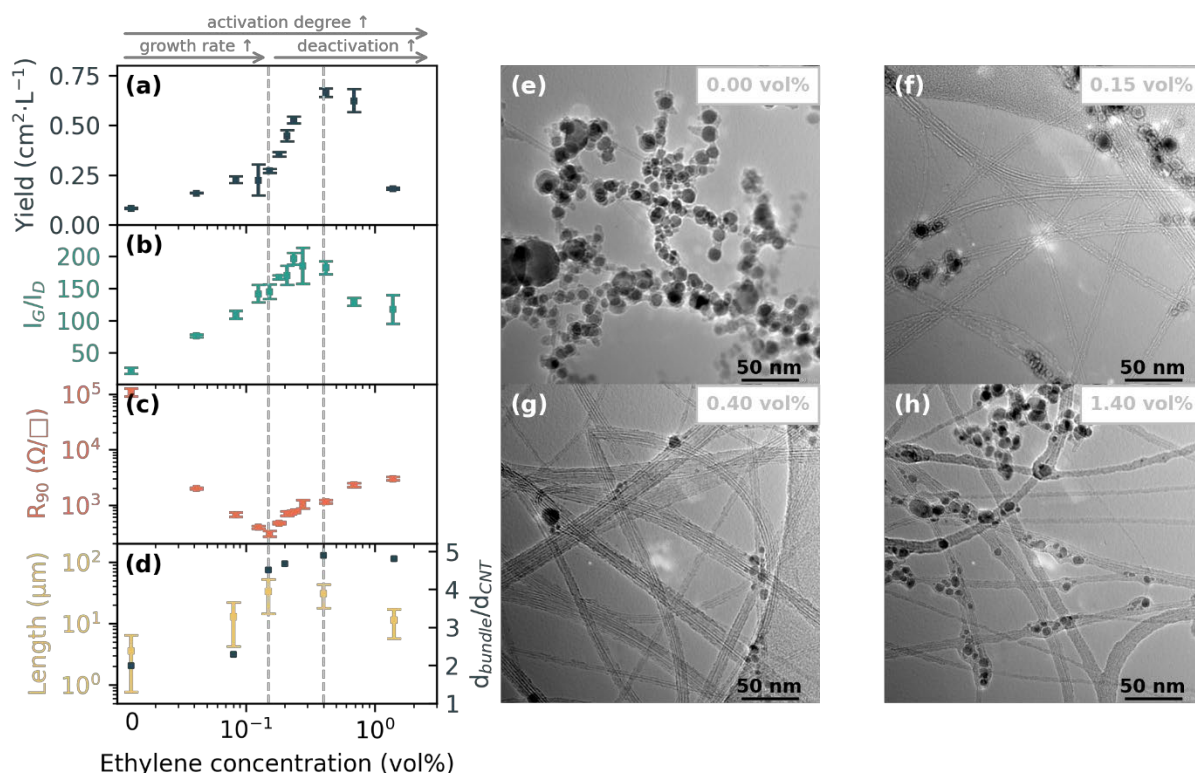


**Figure 4.** The comparison of Yield (a),  $I_G/I_D$  (b),  $R_{90}$  (c), nanotube bundle length, and diameter (d) ethylene concentration dependences (at a ferrocene feed rate of  $43 \mu\text{g}/\text{min}$  and toluene feed rate of  $5.0 \mu\text{l}/\text{min}$ ) and synthesis temperature  $1050^\circ\text{C}$ . (e-k) – TEM micrographs of samples collected at 0, 0.08, 0.15, 0.20, 0.40 and 1.40 vol% ethylene

concentration correspondingly. Here,  $d_{bundle}$  and  $d_{CNT}$  correspond to mean bundle and nanotube diameters, correspondingly.

The results of electronic microscopy observation (**Figure 4(e-h)**) reveal the effect of ethylene on product morphology. According to TEM, ethylene introduction significantly reduces the fraction of non-activated iron catalysts and increases the bundle diameter that is in line with its promoting effect during the nucleation. We consider the ratio of mean bundle diameter to mean nanotube diameter ( $d_{bundle}/d_{CNT}$ ; **Figure 4d**) as a characteristic value for the catalyst activation degree. Indeed, at a fixed residence time, the bundling rate is mainly affected by nanotube concentration in the aerosol phase, which, in turn, is a function of the number of active catalyst nanoparticles. Thus, at a fixed ferrocene feed rate, the catalyst activation degree governs the effective number of nanotubes in a bundle ( $d_{bundle}/d_{CNT}$ ). We found  $d_{bundle}/d_{CNT}$  to be a sigmoid-like function of ethylene concentration raising from 2 (without ethylene) to 5 (at 0.4 vol% of ethylene) and being nearly constant at higher concentrations. We believe the further growth of catalyst activation degree ( $d_{bundle}/d_{CNT}$ ) is inhibited by a higher supersaturation of catalyst with carbon required for formation of a low diameter SWCNT nuclei according to nucleation theory ([45]). Thus, we may conclude the ethylene to act as an activation agent significantly enhancing catalyst utilization degree in  $C_2H_4$  concentration range studied.

Moreover, we investigated the bundle length statistics describing growth efficiency as a function of grow rate and catalyst lifetime by SEM. Surprisingly, we found a significant effect of ethylene concentration on the mean bundle length. The nanotube bundle length shows a bell-shaped relation with ethylene concentration, reaching maxima of 33  $\mu m$  at 0.15 vol% of ethylene. The coincidence of the length increase with the  $R_{90}$  reduction confirms the fundamental role of nanotube bundle length in film transparent and conductive properties [16]. Besides, we observed similar trends for the mean bundle length and  $I_G/I_D$  with ethylene concentration coincides with the theory of defect formation predominantly during the nucleation stage [46], since higher nanotube length corresponds to lower defect concentration (defects are predominantly localized at the

edges). In fact, implementing SEM spectroscopy we could not distinguish individual nanotubes and bundles. Though, supporting the mean bundle length statistics by TEM data on bundling we may assess the nanotube length. The observed range of changes for the bundle diameter (2-3 times change) is significantly lower than that one for the bundle length (10-fold change), indicating the pivotal effect of nanotube length. However, other indirect approaches *e.g.* based on viscosity measurements of nanotube dispersions in super acid might be used for length assessment [47]. But we believe this method is of limited use for reliable and unambiguous SWCNT length determination, especially considering the accompanied changes in nanotube morphology, diameter, *etc.*

A dramatic increase in  $R_{90}$  with ethylene concentrations above 0.15 vol% (despite high mean bundle length) is related to the nanotube bundling (induced by enhanced catalyst activation degree), followed by the length decrease revealing an inhibiting role of ethylene at higher concentrations. The latter effect might be caused by the catalyst poisoning by carbon – one of the main reasons of catalyst deactivation during aerosol CVD synthesis [48]. Comparing the yield data with bundle length and diameter data, we may attribute an increase in yield at concentrations below 0.4 vol% to activation degree and growth-rate (<0.15 vol%) enhancement, while the further decline is presumably associated with carbon poisoning by excessive ethylene concentration (despite the high activation degree).

To sum up, we found the ethylene to affect both activation of the Fe-based catalyst and SWCNT growth rate proving its essential role in synthesis tuning. Ethylene facilitates **SWCNT nucleation** at the concentrations studied:

- boosts SWCNT nucleation by the lower critical radius of nanotube nucleus (thinner diameter of nanotubes) and widening the diameter distribution
- promotes catalyst activation degree (the increase of  $d_{\text{bundle}}/d_{\text{CNT}}$ ; the lower amount of inactive particle on TEM; the indirect increase of the yield)

### Ethylene affects SWCNT growth rate:

- enhances the growth rate at concentrations below 0.15 vol% (increase in SWCNT length; the indirect increase of the yield and nanotube quality ( $I_G/I_D$ ); the indirect decrease of  $R_{90}$ );
- inhibits the growth (early deactivation) at higher concentrations (decrease in SWCNT length; the indirect decrease of the yield and nanotube quality ( $I_G/I_D$ ); indirect increase of  $R_{90}$ ).

### 3.3 Effect of toluene

In contrast to fundamental role of ethylene, which was discussed previously, in the pioneer works, toluene was considered as the main carbon feedstock [42,49] for the studied system, enabling synthesis of wide diameter ( $>2.2$  nm; **Figure 3**) SWCNTs at high growth rates. The reactor design allows us to exclude ethylene effect and directly investigate the performance of toluene as the only carbon source.

**Figure 5** uncovers the influence of toluene feed rate on the main output characteristics of produced SWCNT films at different ferrocene feed rates. Overall, evaluating the toluene as individual (without ethylene addition) feedstock, we found the increase in its concentration enhances both the quality of produced films (**Figure 5c**) and their optoelectronic properties (**Figure 5e**). In fact, we observed 3-fold improvement of  $I_G/I_D$  (from 50 to 150) and two-order of magnitude  $R_{90}$  enhancement in the investigated concentration regions that is comparable with the results of ethylene concentration adjustment. The simultaneous improvement of  $I_G/I_D$  and  $R_{90}$  might be related to the increase in nanotube length (by the analogy with arguments given in previous section) and indicates the growth-rate enhancing role of toluene.

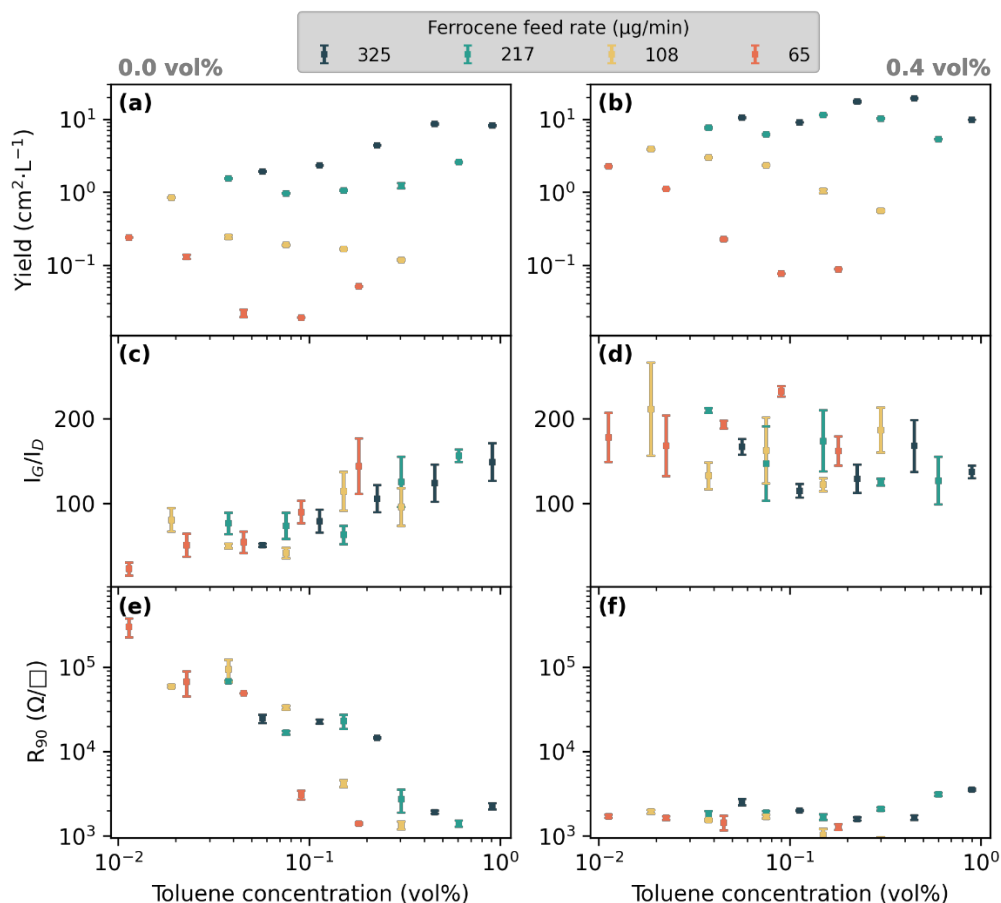


**Figure 5.** The effect of toluene feed rate on nanotube film characteristics at 0 (a,c,e) and 0.4 vol% (b,d,f) ethylene concentrations.

On the contrary, the ethylene addition results in a less pronounced effect of toluene both on nanotube defectiveness and material conductivity (**Figure 5d,f**) that supports either role of ethylene as the main carbon source for SWCNTs or toluene role as an inhibitor of catalyst activation. Indeed, we observed an ambiguous influence of toluene on the synthesis productivity (**Figure 5a,b**) independent of the ethylene concentration. At a high ferrocene feed rate (325 μg/min), we found an upward trend of the synthesis productivity with toluene concentration. When decreasing the ferrocene feed rate, we first observed less noticeable yield improvement (at 217 μg/min) by the toluene, which eventually changed to a declining trend at lower ferrocene feed rates (65 and 108 μg/min). It should be mentioned that considering the lack of any changes in R<sub>90</sub> with toluene addition under any catalyst concentration, we believe the yield to be mostly affected not by the growth rate but the activation degree of the catalyst [24].

The obtained results indicate that optimal toluene concentration strongly depends on the amount of catalyst introduced (or even labile ferrocene hydrocarbon residuals [37]), and an excess of toluene may inhibit the growth. Indeed, analogously with results obtained previously with acetylene/ortho-xylene system [50], an excess of toluene byproducts on the catalyst surface may have growth-inhibiting effect. In particular, we consider that presence of relatively stable toluene decomposition products on catalyst surface decreases catalyst activity at early growth stages. As a result, toluene limits carbon feed rate to the catalyst, deteriorating its activation degree.

### 3.4 *The interplay between carbon feedstock concentrations*

The effects associated with toluene feed rate might also be displayed by its interplay with ethylene concentration. **Figure 6** demonstrates the joint effect of ethylene and toluene on the properties of SWCNTs produced at a fixed ferrocene feed rate. Surprisingly, we found the synthesis productivity (Yield; **Figure 6a**) to be significantly improved at low toluene concentrations compared to higher ones regardless of ethylene concentration (shown in **Figure 5**). This effect is also accompanied by a more pronounced ethylene concentration dependence of yield at low toluene concentrations spanning from 0.12 to 2.78 cm<sup>2</sup>·L<sup>-1</sup> at 0.01 vol% of toluene since at these conditions, ethylene is considered as the main carbon feedstock.

We also found a similar pattern for both R<sub>90</sub> and I<sub>G</sub>/I<sub>D</sub> contour plots (**Figure 6b** and **c**) with fundamental ethylene effect at low toluene concentrations (3 order of magnitude R<sub>90</sub> variation at 0.01 vol% of toluene) and flattening of corresponding relations at high concentrations. On the other hand, at low ethylene concentrations, toluene serves as the main carbon source resulting in R<sub>90</sub> (two-order of magnitude decrease) and I<sub>G</sub>/I<sub>D</sub> (from 20 to 180) improvement. Indeed, at high (>0.1 vol%) toluene concentrations, high material crystallinity (I<sub>G</sub>/I<sub>D</sub>) and conductive properties (R<sub>90</sub>) are observed even at low ethylene concentrations that highlight the interchange effect of toluene and ethylene as carbon feedstock. This hypothesis is also in agreement with a slight downshift in optimal ethylene concentration with the toluene concentration increase, especially noticeable on I<sub>G</sub>/I<sub>D</sub> contour plot (**Figure 6c**). It is worth mentioning that we revealed a beneficial

effect of toluene on  $I_G/I_D$  even at optimal ethylene concentrations since an increase in  $I_G/I_D$  reaching maxima at 0.1 vol% toluene concentration is observed. Thus, high toluene stability might also result in lower nanotube defectiveness compared to ethylene leading to the lower sheet resistance of the films.

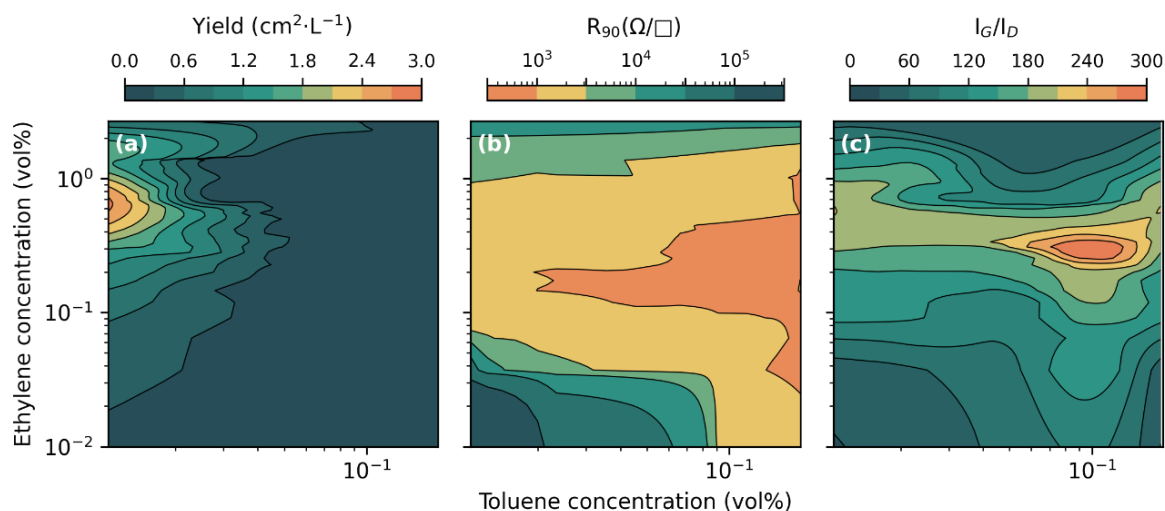


**Figure 6.** The toluene and ethylene interplay illustrated by Yield (a)  $R_{90}$  (b) and  $I_G/I_D$  (c) contour plots. The ferrocene feed rate was fixed at 65  $\mu\text{g}/\text{min}$ .

However, the detrimental effect of toluene on synthesis productivity indirectly confirms our previous hypothesis related to catalyst passivation. This may also explain the less pronounced effect of ethylene at high toluene concentrations since catalyst passivation prevents activation degree promotion by ethylene. However, despite the negative impact of toluene on synthesis, productivity adjustment of toluene concentration also improves the transparent and conductive characteristics of the material as well as results in higher nanotube crystallinity. Perhaps, the toluene effect on nanotube yield may improve at higher growth temperatures (>1100°C, Figure S8); though, high-temperature synthesis process is more technologically complicated from the perspective of reactor design and energy effectiveness. Thus, despite its inhibiting role in joint  $\text{C}_2\text{H}_4/\text{C}_7\text{H}_8$  synthesis, toluene contributes as a quality promotor boosting the TCF applications.

### 3.5 Transparent and conductive film performance

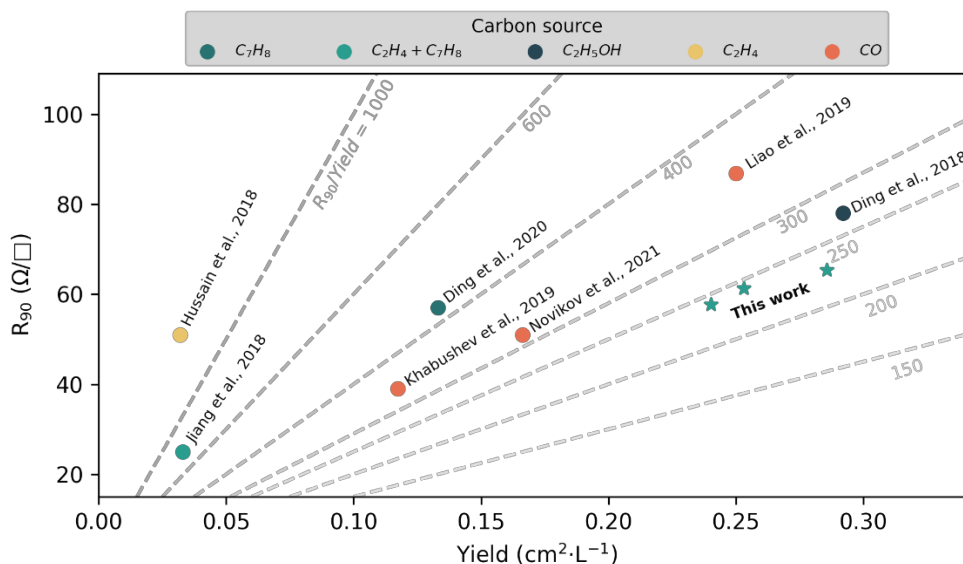


**Figure 7.** The current advances in the field of TCFs of doped SWCNT films produced by aerosol CVD in terms of  $R_{90}$  and Yield [18,29–31,51–53]. Colors mark carbon feedstocks used; results of this work are denoted as stars.

Based on the results of our systematic study, we managed to synthesize nanotube films with low  $R_{90}$  (as low as 300  $\Omega/\square$  in pristine condition; **Figure 4c**) and relatively high yield even implementing low feed rate (5  $\mu\text{l}/\text{min}$ , 0.15-0.20 vol% ethylene concentration) of 1 wt% catalyst solution. However, the performance of pristine nanotube-based transparent conductors is not competitive, and the doping procedure is usually employed to enhance film performance, since it significantly improves the equivalent sheet resistance reducing the contribution of inter-tube junctions (Schottky-barriers) in conductivity. Employing a highly efficient doping technique based on  $\text{HAuCl}_4$  solution [54], we evaluated the TCF performance of the produced material. For this, we analyzed the previously reported data for SWCNT-based transparent conductive films produced implementing aerosol (floating-catalyst) CVD approach using different carbon feedstocks and plotted it in Yield- $R_{90}$  coordinates (**Figure 7**) together with our results.

Overall, the collected data highlights the phenomenological trade-off rule between material yield and TCF performance ( $R_{90}$ ). The observed trend is presumably related to the fundamental limitation of aerosol CVD associated with gas-phase nanotube bundling at high nanotube concentrations in aerosol (high yield), deteriorating the TCF performance. It is worth mentioning

that we also observed clustering of results achieved with different carbon feed stocks (*e.g.* CO, marked by orange in **Figure 7**). This fact might be related to the fundamental influence of carbon feedstock on the growth rate and, as follows, on the length of produced nanotubes (affecting both  $R_{90}$  and Yield parameters). Besides, according to the provided comparison, one can conclude that implementing several carbon feedstocks is beneficial from the perspective of  $R_{90}$  and Yield trade-off. Thus, the results achieved combining toluene and ethylene as carbon feedstocks reveal significant improvement in the yield next to results reported with ethylene (14-fold) and toluene (2-fold) alone for the films with comparable  $R_{90}$  values (51-57  $\Omega/\square$ ).

#### 4. Conclusion

In summary, we have systematically investigated the SWCNT synthesis by aerosol CVD varying ethylene and toluene as the carbon sources. Having inspected the effects of synthesis parameters (ferrocene feed rate, ethylene, and toluene concentration) on the characteristics of produced material, we claim the role of ethylene not only to tune the diameter of the produced SWCNTs (as reported before) but also to improve the catalyst activation degree and nanotube growth rate significantly. Besides, the excessive ethylene concentrations deteriorate both the synthesis productivity and film characteristics because of catalyst poisoning by carbon.

On the contrary, toluene, being a more stable molecule than ethylene, inhibits catalyst activation degree resulting in reduced yield of SWCNTs. Even more, as the only carbon source, toluene was shown to hardly activate the Fe-based catalyst, presumably due to lower supersaturation levels of the iron catalyst with carbon provided by toluene. Nevertheless, the lower reaction rates for carbon intermediates of toluene decomposition promote the nanotube crystallinity (decreases defectiveness), leading under certain conditions to lower  $R_{90}$ .

**Table 2.** The overall influence of synthesis parameters on characteristics of produced SWCNT films.

	$d_{CNT}$	Yield	$I_G/I_D$	$R_{90}$	Role
Cat. feed rate	↑	↑	↓	↑	Improves activation degree and process productivity

Ethylene conc.	↓	↗0.4vol%↘	↗0.4vol%↘	↘0.1-0.2vol%↗	Promotes activation and increases growth rate (<0.15 vol%) while leading to earlier deactivation at higher concentrations
Toluene conc.	↓	↓	↑	↓	Increases growth rate w/o C <sub>2</sub> H <sub>4</sub> , decreases activation degree; reduces carbon feed rate to catalyst boosting crystallinity

Adjusting synthesis conditions, we fabricated samples with the equivalent resistance value of  $57 \Omega/\square$  after H<sub>2</sub>AuCl<sub>4</sub> doping and a relatively high yield of  $0.24 \text{ cm}^2 \cdot \text{L}^{-1}$  that exceed in several times the previous results achieved with ethylene and toluene independently. We believe our work to contribute to the understanding of carbon feedstock effects in carbon nanotube growth by aerosol CVD and to promote further progress in the field of high yield production of nanotube-based transparent and conductive films.

### Acknowledgements

The authors thank Anton Bubis and MIPT Shared Facilities Center for the help with scanning electron microscopy. E.M.Kh. and D.V.K. acknowledge Russian Science Foundation grant No. 20-73-10256 (synthesis of SWCNTs and optical measurements). E.M.Kh. and T.K. acknowledge Academy of Finland project No. 320167 (PREIN Flagship - Aalto University). Q.Zh. and E.I.K. acknowledge Academy of Finland project No. 316572 (CNTstress). A.G.N. and A.E.G. acknowledge the Russian Science Foundation (project No. 17-19-01787 - doping of carbon nanotubes). E.I.K. acknowledge the Academy of Finland for Mobility Grant (application number 334466). A.P.Ts. acknowledges the EDUFI Fellowship (No. TM-19-11079) from the Finnish National Agency for Education and the Magnus Ehrnrooth Foundation (the Finnish Society of Sciences and Letters) for personal financial support. This work made use of the Aalto University Otanano, RAMI and Bioeconomy infrastructures.

## References

- [1] A.G. Nasibulin, A. Kaskela, K. Mustonen, A.S. Anisimov, V. Ruiz, S. Kivistö, S. Rackauskas, M.Y. Timmermans, M. Pudas, B. Aitchison, M. Kauppinen, D.P. Brown, O.G. Okhotnikov, E.I. Kauppinen, Multifunctional free-standing single-walled carbon nanotube films, *ACS Nano*. 5 (2011) 3214–3221. doi:10.1021/nn200338r.
- [2] M. Bersanelli, Controversies about COVID-19 and anticancer treatment with immune checkpoint inhibitors, *Immunotherapy*. 12 (2020) 269–273. doi:10.2217/imt-2020-0067.
- [3] D.M. Sun, M.Y. Timmermans, Y. Tian, A.G. Nasibulin, E.I. Kauppinen, S. Kishimoto, T. Mizutani, Y. Ohno, Flexible high-performance carbon nanotube integrated circuits, *Nat. Nanotechnol.* 6 (2011) 156–161. doi:10.1038/nnano.2011.1.
- [4] M.Y. Timmermans, D. Estrada, A.G. Nasibulin, J.D. Wood, A. Behnam, Effect of Carbon Nanotube Network Morphology on Thin Film Transistor Performance, 5 (2012) 307–319. doi:10.1007/s12274-012-0211-8.
- [5] P. et al. Avouris, The role of metal-NT contact in the performance of CNFETs, *Nano Lett.* 5 (2005) 1497–502. <http://www.ncbi.nlm.nih.gov/pubmed/16178264>.
- [6] D.S. Kopylova, F.S. Fedorov, A.A. Alekseeva, E.P. Gilshteyn, A.P. Tsapenko, A. V. Bubis, A.K. Grebenko, Z.I. Popov, P.B. Sorokin, Y.G. Gladush, A.S. Anisimov, A.G. Nasibulin, Holey single-walled carbon nanotubes for ultra-fast broadband bolometers, *Nanoscale*. 10 (2018) 18665–18671. doi:10.1039/c8nr05925j.
- [7] S.A. Romanov, A.E. Aliev, B. V. Fine, A.S. Anisimov, A.G. Nasibulin, Highly efficient thermophones based on freestanding single-walled carbon nanotube films, *Nanoscale Horizons*. 4 (2019) 1158–1163. doi:10.1039/c9nh00164f.
- [8] L. Yu, C. Shearer, J. Shapter, Recent Development of Carbon Nanotube Transparent Conductive Films, *Chem. Rev.* 116 (2016) 13413–13453.

doi:10.1021/acs.chemrev.6b00179.

- [9] S. Qu, Y. Dai, D. Zhang, Q. Li, T.W. Chou, W. Lyu, Carbon nanotube film based multifunctional composite materials: An overview, *Funct. Compos. Struct.* 2 (2020). doi:10.1088/2631-6331/ab9752.
- [10] I. Dierking, Carbon Allotropes as ITO Electrode Replacement Materials in Liquid Crystal Devices, *C.* 6 (2020) 80. doi:10.3390/c6040080.
- [11] S.H. Chae, Y.H. Lee, Carbon nanotubes and graphene towards soft electronics, *Nano Converg.* 1 (2014) 1–26. doi:10.1186/s40580-014-0015-5.
- [12] E. Gilshteyn, S. Romanov, D. Kopylova, G. Savostyanov, A. Anisimov, O. Glukhova, A. Nasibulin, Mechanically Tunable Single-Walled Carbon Nanotube Films as a Universal Material for Transparent and Stretchable Electronics, *ACS Appl. Mater. Interfaces.* 11 (n.d.) 27327–27334. doi:10.1021/acsami.9b07578.
- [13] A.G. Nasibulin, A. Moisala, D.P. Brown, H. Jiang, E.I. Kauppinen, A novel aerosol method for single walled carbon nanotube synthesis, *Chem. Phys. Lett.* 402 (2005) 227–232. doi:10.1016/j.cplett.2004.12.040.
- [14] R. Rao, C.L. Pint, A.E. Islam, R.S. Weatherup, S. Hofmann, E.R. Meshot, F. Wu, C. Zhou, N. Dee, P.B. Amama, J. Carpena-Nuñez, W. Shi, D.L. Plata, E.S. Penev, B.I. Yakobson, P.B. Balbuena, C. Bichara, D.N. Futaba, S. Noda, H. Shin, K.S. Kim, B. Simard, F. Mirri, M. Pasquali, F. Fornasiero, E.I. Kauppinen, M. Arnold, B.A. Cola, P. Nikolaev, S. Arepalli, H.M. Cheng, D.N. Zakharov, E.A. Stach, J. Zhang, F. Wei, M. Terrones, D.B. Geohegan, B. Maruyama, S. Maruyama, Y. Li, W.W. Adams, A.J. Hart, Carbon Nanotubes and Related Nanomaterials: Critical Advances and Challenges for Synthesis toward Mainstream Commercial Applications, *ACS Nano.* 12 (2018) 11756–11784. doi:10.1021/acsnano.8b06511.

- [15] J. Du, S. Pei, L. Ma, H.M. Cheng, 25th anniversary article: Carbon nanotube- and graphene-based transparent conductive films for optoelectronic devices, *Adv. Mater.* 26 (2014) 1958–1991. doi:10.1002/adma.201304135.
- [16] A. Kaskela, A.G. Nasibulin, M.Y. Timmermans, B. Aitchison, A. Papadimitratos, Y. Tian, Z. Zhu, H. Jiang, D.P. Brown, A. Zakhidov, E.I. Kauppinen, Aerosol-synthesized SWCNT networks with tunable conductivity and transparency by a dry transfer technique, *Nano Lett.* 10 (2010) 4349–4355. doi:10.1021/nl101680s.
- [17] Q. Zhang, N. Wei, P. Laiho, E.I. Kauppinen, Recent Developments in Single-Walled Carbon Nanotube Thin Films Fabricated by Dry Floating Catalyst Chemical Vapor Deposition, *Top. Curr. Chem.* 375 (2017) 99–128. doi:10.1007/s41061-017-0178-8.
- [18] Y. Liao, A. Hussain, P. Laiho, Q. Zhang, Y. Tian, N. Wei, E.X. Ding, S.A. Khan, N.N. Nguyen, S. Ahmad, E.I. Kauppinen, Tuning Geometry of SWCNTs by CO<sub>2</sub> in Floating Catalyst CVD for High-Performance Transparent Conductive Films, *Adv. Mater. Interfaces.* 5 (2018) 1–10. doi:10.1002/admi.201801209.
- [19] W. Ren, F. Li, S. Bai, H.M. Cheng, The effect of sulfur on the structure of carbon nanotubes produced by a floating catalyst method, *J. Nanosci. Nanotechnol.* 6 (2006) 1339–1345. doi:10.1166/jnn.2006.301.
- [20] B. Yu, C. Liu, P.-X. Hou, Y. Tian, S. Li, B. Liu, F. Li, E.I. Kauppinen, H. Cheng, Bulk Synthesis of Large Diameter Semiconducting Single-Walled Carbon Nanotubes by Oxygen-Assisted Floating Catalyst Chemical Vapor Deposition, *J. Am. Chem. Soc.* 133 (2011) 5232–5235. doi:10.1021/ja2008278.
- [21] U. Khalilov, C. Vets, E.C. Neyts, Molecular evidence for feedstock-dependent nucleation mechanisms of CNTs, *Nanoscale Horizons.* 4 (2019) 674–682. doi:10.1039/c8nh00323h.
- [22] B. McLean, E.I. Kauppinen, A.J. Page, Initial competing chemical pathways during floating

- catalyst chemical vapor deposition carbon nanotube growth, *J. Appl. Phys.* 044302 (2021). doi:10.1063/5.0030814.
- [23] J.S. Barnard, C. Paukner, K.K. Koziol, The role of carbon precursor on carbon nanotube chirality in floating catalyst chemical vapour deposition, *Nanoscale*. 8 (2016) 17262–17270. doi:10.1039/C6NR03895F.
- [24] E.M. Khabushev, D.V. Krasnikov, J.V. Kolodiaznaia, A.V. Bubis, A.G. Nasibulin, Structure-dependent performance of single-walled carbon nanotube films in transparent and conductive applications, *Carbon N. Y.* 161 (2020). doi:10.1016/j.carbon.2020.01.068.
- [25] D. Mitin, Y. Berdnikov, A. Vorobyev, A. Mozharov, S. Raudik, O. Koval, V. Neplokh, E. Moiseev, D. Ilatovskii, A.G. Nasibulin, I. Mukhin, Optimization of Optoelectronic Properties of Patterned Single-Walled Carbon Nanotube Films, *ACS Appl. Mater. Interfaces*. 12 (2020) 55141–55147. doi:10.1021/acsami.0c14783.
- [26] K. Mustonen, P. Laiho, A. Kaskela, T. Susi, A.G. Nasibulin, E.I. Kauppinen, Uncovering the ultimate performance of single-walled carbon nanotube films as transparent conductors, *Appl. Phys. Lett.* 107 (2015) 1–6. doi:10.1063/1.4932942.
- [27] S.D. Shandakov, A. V. Kosobutsky, M.S. Rybakov, O.G. Sevostyanov, D.M. Russakov, M. V. Lomakin, A.I. Vershinina, I.M. Chirkova, Effect of gaseous and condensate products of ethanol decomposition on aerosol CVD synthesis of single-walled carbon nanotubes, *Carbon N. Y.* 126 (2018) 522–531. doi:10.1016/j.carbon.2017.10.064.
- [28] I. V. Anoshkin, A.G. Nasibulin, Y. Tian, B. Liu, H. Jiang, E.I. Kauppinen, Hybrid carbon source for single-walled carbon nanotube synthesis by aerosol CVD method, *Carbon N. Y.* 78 (2014) 130–136. doi:10.1016/j.carbon.2014.06.057.
- [29] S. Jiang, P.X. Hou, M.L. Chen, B.W. Wang, D.M. Sun, D.M. Tang, Q. Jin, Q.X. Guo, D.D. Zhang, J.H. Du, K.P. Tai, J. Tan, E.I. Kauppinen, C. Liu, H.M. Cheng, Ultrahigh-

- performance transparent conductive films of carbon-welded isolated single-wall carbon nanotubes, *Sci. Adv.* 4 (2018). doi:10.1126/sciadv.aap9264.
- [30] A. Hussain, Y. Liao, Q. Zhang, E. Ding, P. Laiho, S. Ahmad, N. Wei, Y. Tian, H. Jiang, E.I. Kauppinen, Floating catalyst CVD synthesis of single walled carbon nanotubes from ethylene for high performance transparent electrodes, *Nanoscale*. 10 (2018) 9752–9759. doi:10.1039/C8NR00716K.
- [31] E.-X. Ding, A. Hussain, S. Ahmad, Q. Zhang, Y. Liao, H. Jiang, E.I. Kauppinen, High-performance transparent conducting films of long single-walled carbon nanotubes synthesized from toluene alone, *Nano Res.* 13 (2020) 112–120. doi:10.1007/s12274-019-2581-7.
- [32] P.A. Thrower, ed., *Chemistry & Physics of Carbon*, 19th ed., CRC Press, 1984.
- [33] A. Kaskela, A. Nasibulin, M. Zavodchikova, B. Aitchison, A. Papadimitratos, Y. Tian, Z. Zhu, H. Jiang, D. Brown, A. Zakhidov, E. Kauppinen, Aerosol-Synthesized SWCNT Networks with Tunable Conductivity and Transparency by a Dry Transfer Technique, *Nano Lett.* 10 (n.d.) 4349–4355. doi:10.1021/nl101680s.
- [34] V.Y. Iakovlev, D. V Krasnikov, E.M. Khabushev, J. V Kolodiaznaia, Artificial neural network for controlled synthesis of single-walled carbon nanotubes by aerosol CVD method, 153 (2019) 1–6. doi:10.1016/j.carbon.2019.07.013.
- [35] H. Kataura, Y. Kumazawa, Y. Maniwa, I. Umezumi, S. Suzuki, Y. Ohtsuka, Y. Achiba, Optical properties of single-wall carbon nanotubes, *Synth. Met.* 103 (1999) 2555–2558. doi:10.1016/S0379-6779(98)00278-1.
- [36] O. Reynaud, A.G. Nasibulin, A.S. Anisimov, I. V. Anoshkin, H. Jiang, E.I. Kauppinen, Aerosol feeding of catalyst precursor for CNT synthesis and highly conductive and transparent film fabrication, *Chem. Eng. J.* 255 (2014) 134–140.

doi:10.1016/j.cej.2014.06.082.

- [37] V.Y. Iakovlev, D. V. Krasnikov, E.M. Khabushev, A.A. Alekseeva, A.K. Grebenko, A.P. Tsapenko, B.Y. Zabelich, J. V. Kolodiaznaia, A.G. Nasibulin, Fine-tuning of spark-discharge aerosol CVD reactor for single-walled carbon nanotube growth: The role of ex situ nucleation, *Chem. Eng. J.* (2019) 123073. doi:10.1016/j.cej.2019.123073.
- [38] A.G. Nasibulin, P. V. Pikhitsa, H. Jiang, E.I. Kauppinen, Correlation between catalyst particle and single-walled carbon nanotube diameters, *Carbon N. Y.* 43 (2005) 2251–2257. doi:10.1016/j.carbon.2005.03.048.
- [39] S. Hofmann, R. Sharma, C. Ducati, G. Du, C. Mattevi, C. Cepek, M. Cantoro, S. Pisana, A. Parvez, F. Cervantes-Sodi, A.C. Ferrari, R. Dunin-Borkowski, S. Lizzit, L. Petaccia, A. Goldoni, J. Robertson, In situ Observations of Catalyst Dynamics during Surface-Bound Carbon Nanotube Nucleation, *Nano Lett.* 7 (2007) 602–608. doi:10.1021/nl0624824.
- [40] V.Y. Iakovlev, D.V. Krasnikov, E.M. Khabushev, A.A. Alekseeva, A.K. Grebenko, A.P. Tsapenko, B.Y. Zabelich, J.V. Kolodiaznaia, A.G. Nasibulin, Fine-tuning of spark-discharge aerosol CVD reactor for single-walled carbon nanotube growth: The role of ex situ nucleation, *Chem. Eng. J.* 383 (2020). doi:10.1016/j.cej.2019.123073.
- [41] V. Jourdain, C. Bichara, Current understanding of the growth of carbon nanotubes in catalytic chemical vapour deposition, *Carbon N. Y.* 58 (2013) 2–39. doi:10.1016/j.carbon.2013.02.046.
- [42] T. Saito, S. Ohshima, T. Okazaki, S. Ohmori, M. Yumura, S. Iijima, Selective Diameter Control of Single-Walled Carbon Nanotubes in the Gas-Phase Synthesis, 8 (2008) 6153–6157. doi:10.1166/jnn.2008.SW23.
- [43] E.M. Khabushev, D. V. Krasnikov, J. V. Kolodiaznaia, A. V. Bubis, A.G. Nasibulin, Structure-dependent performance of single-walled carbon nanotube films in transparent and

- conductive applications, *Carbon N. Y.* 161 (2020) 712–717. doi:10.1016/j.carbon.2020.01.068.
- [44] D. Hecht, L. Hu, G. Grüner, Conductivity scaling with bundle length and diameter in single walled carbon nanotube networks, *Appl. Phys. Lett.* 89 (2006) 1–4. doi:10.1063/1.2356999.
- [45] V.L. Kuznetsov, A.N. Usoltseva, A.L. Chuvilin, E.D. Obraztsova, Thermodynamic analysis of nucleation of carbon deposits on metal particles and its implications for the growth of carbon nanotubes, 64 (2001) 1–7. doi:10.1103/PhysRevB.64.235401.
- [46] Y. Ohta, Y. Okamoto, S. Irle, K. Morokuma, Rapid growth of a single-walled carbon nanotube on an iron cluster: Density-functional tight-binding molecular dynamics simulations, *ACS Nano.* 2 (2008) 1437–1444. doi:10.1021/nn8001906.
- [47] D.E. Tsentalovich, A.W.K. Ma, J.A. Lee, N. Behabtu, E.A. Bengio, A. Choi, J. Hao, Y. Luo, R.J. Headrick, M.J. Green, Y. Talmon, M. Pasquali, Relationship of Extensional Viscosity and Liquid Crystalline Transition to Length Distribution in Carbon Nanotube Solutions, *Macromolecules.* 49 (2016) 681–689. doi:doi.org/10.1021/acs.macromol.5b02054.
- [48] A.S. Anisimov, A.G. Nasibulin, H. Jiang, P. Launois, J. Cambedouzou, S.D. Shandakov, E.I. Kauppinen, Mechanistic investigations of single-walled carbon nanotube synthesis by ferrocene vapor decomposition in carbon monoxide, *Carbon N. Y.* 48 (2009) 380–388. doi:10.1016/j.carbon.2009.09.040.
- [49] H. Ago, S. Ohshima, K. Uchida, M. Yumura, Gas-phase synthesis of single-wall carbon nanotubes from colloidal solution of metal nanoparticles, *J. Phys. Chem. B.* 105 (2001) 10453–10456. doi:10.1021/jp012084j.
- [50] Y. Ma, A.B. Dichiara, D. He, L. Zimmer, J. Bai, Control of product nature and morphology by adjusting the hydrogen content in a continuous chemical vapor deposition process for

- carbon nanotube synthesis, *Carbon* N. Y. 107 (2016) 171–179. doi:10.1016/j.carbon.2016.05.060.
- [51] E. Ding, Q. Zhang, N. Wei, A.T. Khan, E.I. Kauppinen, High-performance single-walled carbon nanotube transparent conducting film fabricated by using low feeding rate of ethanol solution, *R. Soc. Open Sci.* 5 (2018) 180392. doi:10.1098/rsos.180392.
- [52] E.M. Khabushev, D. V. Krasnikov, O.T. Zarembo, A.P. Tsapenko, A.E. Goldt, A.G. Nasibulin, Machine Learning for Tailoring Optoelectronic Properties of Single-Walled Carbon Nanotube Films, *J. Phys. Chem. Lett.* 10 (2019) 6962–6966. doi:10.1021/acs.jpcclett.9b02777.
- [53] I. V. Novikov, E.M. Khabushev, D. V. Krasnikov, A. V. Bubis, A.E. Goldt, S.D. Shandakov, A.G. Nasibulin, Residence time effect on single-walled carbon nanotube synthesis in an aerosol CVD reactor, *Chem. Eng. J.* 420 (2021) 129869. doi:10.1016/j.cej.2021.129869.
- [54] A.E. Goldt, O.T. Zarembo, M.O. Bulavskiy, F.S. Fedorov, K. V. Larionov, A.P. Tsapenko, Z.I. Popov, P. Sorokin, A.S. Anisimov, H. Inani, J. Kotakoski, K. Mustonen, A.G. Nasibulin, Highly efficient bilateral doping of single-walled carbon nanotubes, *J. Mater. Chem. C* 9 (2021) 4514–4521. doi:10.1039/D0TC05996J.